Nonlinear modeling of the effect of multiple locked modes on heat transport

Q.M. Hu[1], X.D. Du[2], Q. Yu[3], N.C. Logan[1], E. Kolemen[4], R. Nazikian[1]

[1] *Princeton Plasma Physics Laboratory, Princeton NJ 08543-0451, USA*
[2] *University of California Irvine, Irvine CA 92697, USA*
[3] *Max-Plank-Institut für Plasmaphysik, 85748 Garching, Germany*
[4] *Mechanical and Aerospace Engineering, Princeton University, Princeton NJ, USA*

Extensive studies find that locked modes (LMs) are one of the main causes of disruptions [1, 2]. LMs form locked magnetic island chains at rational surfaces and cause substantial deterioration of energy confinement. Large enough LMs can lead to thermal quenches (TQs) and major disruptions [3, 4]. After one mode locks, multiple LMs with different helicities often grow and coexist [5, 6]. These multiple LMs challenge the study of the transition process from LMs to TQ in both experiment and theory. In the experiment, it is difficult to detect and distinguish multiple locked island chains due to the loss of mode rotation. In theoretical modeling, plasma transport and nonlinear effects in the presence of multiple LMs is computationally expensive. There are many investigations on the transition process from LMs to TQs [7–9], however, this transition process is still poorly understood until now. What is known is that TQs are found to occur when the amplitude of a LM reaches a distinct level and that LMs are precursors to disruptions that enable simple disruption prediction schemes. Therefore, improving the physical understanding of the transition process from LMs to TQs might lead to better disruption prediction and avoidance, which is essential for the success of ITER [3, 4].

In a recent DIII-D experiment, an ohmic $q_{95} \sim 4$ plasma with LMs, due to EF penetration at low electron density, evolves to TQ and terminates by major disruption. By using a dual tangential soft X-ray imaging (DSXI) system, the topology of locked island chains with multiple helicities (m/n = 2/1, 3/1 and 4/1) are observed directly and these island chains govern the cooling process in the plasma peripheral region [6]. There is no error field correction for this shot, and the amplitude of the 2/1, 3/1 and 4/1 EFs at the corresponding rational surfaces are calculated to be 2 G, 1.2 G and 2.1 G by using the SURFMN [10] vacuum code. Fig. 1 presents Thomson Scattering (TS) measurements of electron temperature T_e profiles at different times after EF penetration, here EF penetration happens at t = 5.05 s. A flattening is noticeable in the T_e profile at the q = 2, 3 and 4 locations due to the formation of 2/1, 3/1 and 4/1 locked magnetic islands respectively. As time evolves, the widths of the flattening regions become wider

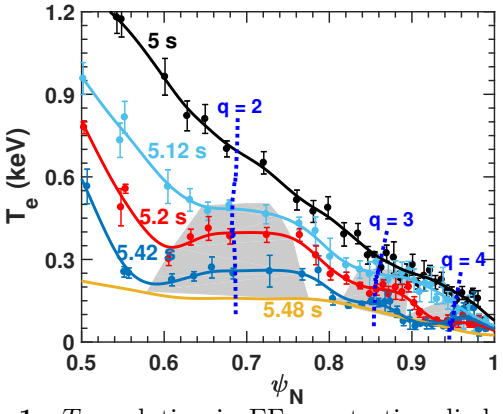

Fig. 1. T_e evolution in EF penetration discharge #172102 measured by Thomson scattering at times t = 5 s, 5.12 s, 5.2 s, 5.42 s and 5.48 s. The position and T_e at q = 2, 3 and 4 rational surfaces are the blue dotted curves, and the shadows show the locked island region derived from T_e profiles.

(the shadows) and T_e at the island region becomes lower due to the growth of the island width. The growing magnetic island gets closer to neighboring ones as indicated by the decreasing boundary distance between the flattening regions. The flattening regions due to 3/1 and 4/1 islands almost overlap prior to the TQ. After the TQ, the T_e profile at 5.48 s is almost flat from the $q = 2$ surface to the plasma edge.

To understand how the multiple LMs affect heat transport, a nonlinear theoretical model TM1 [11, 12] based on reduced MHD equations, including the generalized Ohm's law, the equation of motion and energy transport equation, is utilized to simulate this EF penetration and associated evolution of T_e profile. Dedicated numerical methods are utilized in the code to keep the numerical error low even for high values of magnetic Reynolds number and $\chi_{||}/\chi_{\perp}$. Here, $\chi_{||}$ and $\chi_{\perp}$ are the parallel and perpendicular heat diffusivity. The calculations are for multiple helicity perturbations with $m/n = 2/1$, 3/1 and 4/1, and the perpendicular heat diffusivity and the plasma viscosity are assumed to be at the anomalous transport level of 0.5 m^2/s. The simulations are initialized with the equilibrium prior to EF penetration, corresponding to the 5 s profile in Fig. 1, .

It is well understood that, in the presence of a single island, T_e is flattened due to the extreme anisotropic heat transport. In the modeling, a single 2/1 EF with amplitude of 2.3 G causes field penetration (blue curves in Fig. 2(a) and (b)) at 0.1 s. The 2/1 island grows up quickly and saturates at the width of 11.5 cm at $t = 0.2$ s (Fig. 2(a)). With the growth of 2/1 island, T_e is flattened in the island region and the central T_e is decreased by about 20% (Fig. 2(b)). A single helicity 3/1 (4/1) EF with amplitude of 0.8 G (1.05 G) causes a 3/1 (4/1) island to saturate at the width of 3.5 cm (2 cm) as shown by the red dotted curve (green dashed curve) in Fig. 2(a). The 3/1 (4/1) locked island also causes flattening of T_e profile at its rational surface and 5% (2%) reduction in central T_e (Fig. 2(b)).

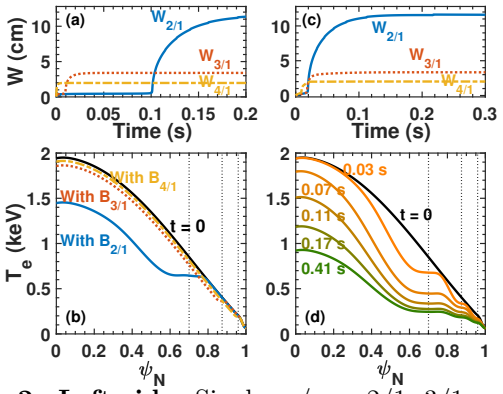

Fig. 2. Left side: Single $m/n = 2/1$, 3/1 or 4/1 EF penetration with (a) time evolution of island width W for $m/n = 2/1$ (blue curve), 3/1 (red dotted curve) and 4/1 (yellow dashed curve), and (b) radial profiles of T_e after locked island saturation.

Right side: EF penetration with $m/n = 2/1$, 3/1 and 4/1 components together. (c) Time evolution of W for $m/n = 2/1$ (blue curve), 3/1 (red dotted curve) and 4/1 (yellow dashed curve), and (d) profiles of T_e at $t = 0$, 0.03 s, 0.07 s, 0.11 s, 0.17 s, 0.41 s. The vertical dotted lines in (b) and (d) indicate the $q = 2$, 3, 4 rational surfaces.

Compared to the single helicity EF penetration cases, $m/n = 2/1$, 3/1 and 4/1 EFs are applied together in Fig. 2(c) with the same amplitude as Fig. 2(a). In this modeling, the EFs are set to ramp up in 20 ms to ensure a clear evolution of the penetration process. It is found that the 4/1 EF penetrates first, followed by 3/1 penetration and finally 2/1 penetration at $t = 0.02$ s. This penetration time is much earlier than in the single 2/1 EF penetration case ($t = 0.1$ s in Fig. 2(a)), indicating multiple helicity EFs accelerate the occurrence of penetration. After the penetration of the 3 helicities, the LMs saturate at the same width as the single helicity cases. In the presence of 2/1, 3/1 and 4/1 LMs,

T_e is flattened at each rational surface, forming a stair-like profile (Fig. 2(d)). Then the profile decreases quickly and globally with the growth of the LMs. In the final saturated state, the central T_e has decreased by more than 50%, which is much higher than the single 2/1 LM case (20%), indicating multiple LMs lead to further reduction of T_e.

Furthermore, after saturation, the T_e profile ranging from $q = 2$ to 4 rational surfaces is nearly flattened even if there is no island overlap evidenced by the magnetic topology as shown in Fig. 3 (b). The detailed evolution of the T_e profile in Fig. 2(d) reveals that the outer edge boundary T_e of the 3/1 locked island is determined by the 4/1 island, and that of the 2/1 locked island is determined by the 3/1 island. This progressive effect on the T_e profile is a unique characteristic of multiple LMs on heat transport, and it is responsible for the much stronger reduction in T_e.

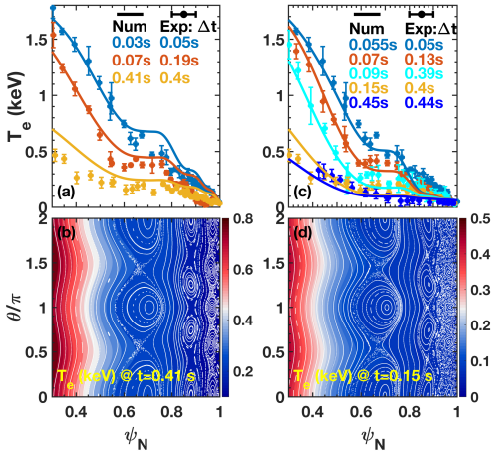

Fig. 3. Left side: From the simulation on the right side of Fig. 2. Comparison of T_e profiles between experiment and modeling (a) at $\Delta t = 0.05$ s, 0.19 s, 0.4 s and $t = 0.03$ s, 0.07 s, 0.41 s, respectively. Modeled 2-D profile of T_e and contour plot of the magnetic topology (b) at $t = 0.41$ s.

Right side: Simulation with experimental 2/1, 3/1 and 4/1 EF amplitudes. Comparison of T_e profiles between experiment and modeling (c) at $\Delta t = 0.05$ s, 0.13 s, 0.39 s, 0.4 s, 0.44 s and $t = 0.055$ s, 0.07 s, 0.09 s, 0.15 s, 0.45 s respectively. Modeled 2-D profile of T_e and flux surfaces (d) at $t = 0.15$ s showing island overlap.

The modeled T_e profiles corresponding to the simulation on the right side of Fig. 2, are compared with experiment in Fig. 3(a). Here, for experiment $\Delta t = t$ - 5.05 s. It is found that the modeled T_e profile is consistent with experiment inside the $q = 2$ surface, but the edge T_e is always higher than the experimental T_e. The global experimental T_e profile just before TQ is also lower than modeled T_e at the new state ($t = 0.41$ s). A possible reason for this discrepency is that the amplitudes of 3/1 and 4/1 EFs in this simulation correspond to the single-helicity penetration thresholds and are lower than the experimental values.

Island overlap happens between 3/1 and 4/1 LMs when applying 2/1, 3/1 and 4/1 EFs with the same amplitudes as in the experiment (Fig. 3(c) and (d)). The modeled T_e profile evolution is quantitatively consistent with experiment (Fig. 3(c)). In this case, the region from the 4/1 locked island to the plasma edge becomes fully stochastic while the 3/1 island chain keeps its complete island structure (Fig. 3(d)). As a result, the T_e profile from the $q = 2$ surface to the plasma edge approaches the plasma edge temperature $T_e(\psi_N = 1)$, leading to full cooling of the plasma in this region.

It should be noted that the redistribution of current density profile due to the change of T_e has not been taken into account in the modeling, since the plasma resistivity as well as the resistive time are held constant at the initial value for the simplification of time normalization. As a result, the time scale of modeled T_e profile evolution is not consistent with experiment. However, it does not matter for the qualitative understanding of the influence of multiple LMs on heat transport.

Further modeling finds that stronger amplitudes of the 2/1, 3/1 and 4/1 EFs drive larger island widths, causing full stochasticity from the 3/1 island region to plasma edge, secondary island structures, and harmonics inside the 2/1 island (Fig. 4). The final T_e profile in such a simulation is even lower than the experimental value after the TQ, indicating that multiple LMs with island overlap can cause enough transport to be responsible for the thermal quench in major disruption.

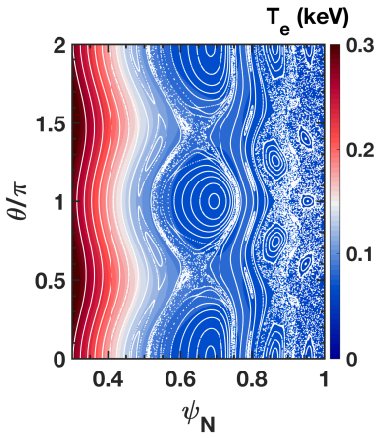

Fig. 4. 2-D profile of T_e and flux surfaces when applying stronger 2/1, 3/1 and 4/1 EFs with amplitude of 5.5 G, 2.1 G and 3.1 G, which lead edge island overlap and secondary island structures.

In summary, the penetration of coexistent $m/n = 2/1$, 3/1 and 4/1 LMs and the resulting effects on heat transport are studied using the nonlinear MHD code TM1. It is found that:

- Multiple helicity EFs accelerate the occurrence of field penetration.
- The coexistence of multiple LMs causes a reduction in T_e ($> 50\%$) that is much higher than in the case of a single 2/1 LM (20%). The coupling of multiple LMs leads to T_e profile that is almost flattened from $q = 2$ to 4 even without island overlap.
- The experimental T_e profile is qualitatively reproduced in the modeling using the experimental EF amplitude. Island overlap happens between 3/1 and 4/1 LMs in this case.
- Stronger EF amplitudes lead to a wider stochastic region, a lower T_e profile, and even secondary island structures.

References

[1] de Vries, P. C. et al., Nuclear Fusion **51** (2011) 053018.
[2] Sweeney, R. et al., Nuclear Fusion **57** (2017) 016019.
[3] ITER Physics Basis Editors, . et al., Nuclear Fusion **39** (1999) 2251.
[4] Hender, T. C. et al., Nuclear Fusion **47** (2007) S128.
[5] Sweeney, R. et al., Nuclear Fusion **58** (2018) 056022.
[6] Du, X. et al., Measurements of the Key Role of Multiple, Small Locked Edge Islands in Triggering Tokamak Disruption, Physical Review Letters 2018 (**submitted**).
[7] Rechester, A. B. et al., Physical Review Letters **40** (1978) 38.
[8] Taylor, P. L. et al., Physical Review Letters **76** (1996) 916.
[9] Fitzpatrick, R., Physics of Plasmas **2** (1995) 825.
[10] Schaffer, M. J. et al., Nuclear Fusion **48** (2008) 024004.
[11] Yu, Q. et al., Physics of Plasmas **10** (2003) 797.
[12] Yu, Q. et al., Nuclear Fusion **48** (2008) 024007.

Disclaimer-This report was prepared as an account of work sponsored by the U.S. Department of Energy under DE-AC02-09CH11466, DE-FOA-0001386, DE-SC0015878 and DE-FC02-04ER546988. Neither the United States Government nor any agency thereof, nor any of their employees, makes any warranty, express or implied, or assumes any legal liability or responsibility for the accuracy, completeness, or usefulness of any information, apparatus, product, or process disclosed, or represents that its use would not infringe privately owned rights. Reference herein to any specific commercial product, process, or service by trade name, trademark, manufacturer, or otherwise, does not necessarily constitute or imply its endorsement, recommendation, or favoring by the United States Government or any agency thereof. The views and opinions of authors expressed herein do not necessarily state or reflect those of the United States Government or any agency thereof. DIII-D data shown in this paper can be obtained in digital format by following the links at https://fusion.gat.com/global/D3D_DMP